



## Geochemical evidence of the sources of aeolian sands and their transport pathways in the Minqin Oasis, northwestern China



Xiaozong Ren<sup>a,b</sup>, Xiaoping Yang<sup>a,\*</sup>, Zhenting Wang<sup>c</sup>, Bingqi Zhu<sup>d</sup>, Deguo Zhang<sup>a</sup>, Patrick Rioual<sup>a</sup>

<sup>a</sup>Key Laboratory of Cenozoic Geology and Environment, Institute of Geology and Geophysics, Chinese Academy of Sciences, Beijing 100029, China

<sup>b</sup>University of Chinese Academy of Sciences, Beijing 100049, China

<sup>c</sup>Cold and Arid Regions Environmental and Engineering Research Institute, Chinese Academy of Sciences, Lanzhou 730000, China

<sup>d</sup>Key Laboratory of Water Cycle and Related Land Surface Processes, Institute of Geographic Sciences and Natural Resources Research, Chinese Academy of Sciences, Beijing 100101, China

### ARTICLE INFO

#### Article history:

Available online 17 May 2014

#### Keywords:

Sand source  
Aeolian process  
Desert  
Oasis  
Geochemistry  
Geomorphology

### ABSTRACT

Identification of aeolian sand sources occurring in oases of desert environments is of great importance for understanding desertification processes and for developing strategies for sustainable development in arid regions. Combined with wind data and hierarchical cluster analysis, we analyzed the spatial characteristics of major and trace elements of sands sampled at the margins of the Minqin Oasis, northwestern China and its adjacent deserts (the Badain Jaran Desert and the Tengger Desert), with the purpose to identify the aeolian sand sources and their transport pathways in the region. The spatial distribution revealed by bivariate plots of Cr, Ni, Cr/V, Y/Ni, Al, V, Zr, Hf, Zr/Hf and ternary plots of major and trace elements showed that sands between the west (B – Badain Jaran Desert, BM – the dune belt between Badain Jaran and the Minqin Oasis and TNE – dune field located in the northeast margin of the Minqin Oasis) and southeast (TSW – dune field located in the southeast margin of the Minqin Oasis) sides of the oasis have different provenances, while the composition of sands in the Minqin Oasis (M) and in the dune field located in the south margin (TM) is associated with both. The variations in abundance of K, Rb, Ba and Sr were used as indicators of aeolian transport processes. Our results show that while aeolian sands from the Badain Jaran Desert can be transported over mountains and over long distances by northwest winds to the west sides of the Minqin Oasis, they cannot directly reach neither bypass the oasis to the east side. Our interpretation is that the oasis can act as an effective barrier to stop the migration of dune fields both in the Badain Jaran Desert and the Tengger Desert. However, the extensive occurrence of aeolian sands in the Minqin Oasis indicates that its role in preventing desert encroachment should not be overestimated.

© 2014 Elsevier Ltd and INQUA. All rights reserved.

### 1. Introduction

Aeolian sand transport, as one of the most important processes involved in the movement and exchange of substance from source zones to depositional sinks, is a direct cause of desertification and also controls the encroachment of sand seas to adjacent areas. Classical aeolian studies have focused partly on the aeolian sand transport (Bagnold, 1941; Kocurek and Lancaster, 1999). Sand transport occurring in deserts reflects changes in desert systems, and as such may provide important reasons why we should better

understand the sand transport pathways and sand sources on regional scales. It is crucial to understand environmental information recorded in sedimentary sequences. Sedimentary sequences contain signals useful for recognizing spatial and temporal changes of deserts and their response to regional or even global climate fluctuations (Yang et al., 2013). In this sense, sedimentary sequences were used widely in the Minqin Basin, Gansu Province, northwestern China (Fig. 1) to interpret the history of climate change (Chen et al., 1999; Zhang et al., 2001, 2002; Long et al., 2012), due to its sensitive location in a climatically interactive zone between the East Asian monsoon and Westerlies domains (Ye, 1990). However, previous studies did not answer the questions of where the aeolian sediments come from and through which pathway they are transported. The Minqin Oasis has attracted

\* Corresponding author.

E-mail addresses: [xpyang@mail.igcas.ac.cn](mailto:xpyang@mail.igcas.ac.cn), [xpyang@263.net.cn](mailto:xpyang@263.net.cn) (X. Yang).

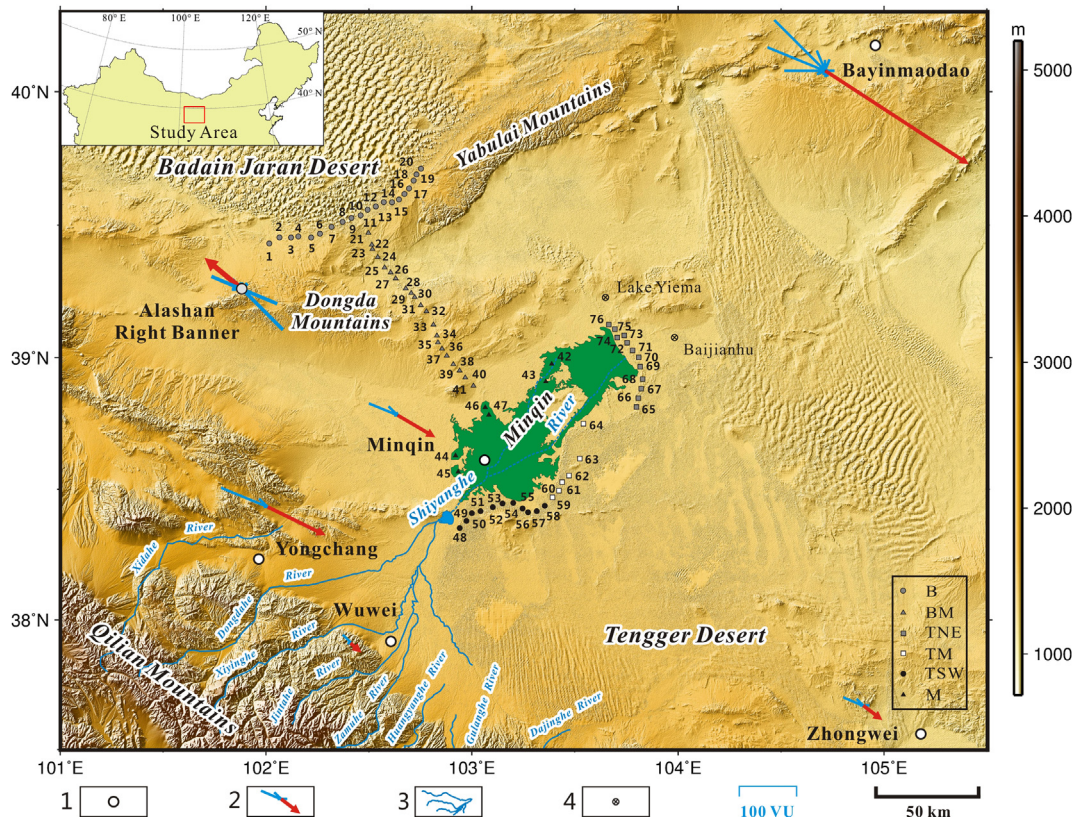


**Fig. 1.** Overview of the study area. B, Sampling sites in the Badain Jaran Desert. BM, Sampling sites along dune belt from the Badain Jaran to the Minqin Oasis. TNE, Sampling sites at the northeastern edge of the oasis. TM, Sampling sites at the southeastern edge of the oasis. TSW, Sampling sites at the southern edge of the oasis. M, Sampling sites in the area of the oasis. 1, Weather stations. 2, Sand rose (Fryberger and Dean, 1979). 3, River. 4, Sedimentary sequences sites. Sand roses for each of the five surrounding weather stations, with blue lines showing winds capable of transporting sand from various directions (DP) and red arrows indicating the resultant sand transport trends (RDP). (For interpretation of the references to colour in this figure legend, the reader is referred to the web version of this article.)

much attention, because it is thought as a “fortress” that prevents merging of two large deserts (the Badain Jaran and Tengger Deserts), as well as reducing the risk of environmental deterioration in this region (Zhang et al., 2005, 2008; Li et al., 2007; Dong et al., 2010). Identification of the transport pathways and sources of the aeolian sands in the Minqin Oasis can help to better understand the mechanism of regional sand transport and help to assess the risk of land degradation.

It is widely accepted that particular geological, geomorphological and climatic conditions have led to substantial transportation and accumulation of dust and loess in northern China (Derbyshire et al., 1998; Smalley et al., 2014). Aeolian sediments from the adjoining gravel and sandy deserts in northern China and southern Mongolia, rather than those from the three large inland desert basins of northwestern China (Tarim, Jungar, and Chaidam), are argued to be the dominant source of loess sediments in the Loess Plateau (Sun, 2002). Determining the sources and transportation of aeolian sediments in the Minqin Basin and adjoining deserts would be helpful for a better understanding of the relationship between loess and deserts in China (Liu, 1985; Sun, 2002; Yang et al., 2007a, 2011).

Numerous and diverse methods are applied to study sand transport, including numerical modelling (Tsoar et al., 1996), field measurement (Lancaster et al., 2002; Ruz and Meur-Ferec, 2004; Wang et al., 2008; Villatoro et al., 2010), remote sensing (Zimelman et al., 1995; Ramsey et al., 1999) and geochemical methods (Muhs et al., 1996a; Pease et al., 1998; Zimelman and Williams, 2002; Muhs et al., 2003; Roy and Smykatz-Kloss,

2007; Yang et al., 2007a; Kasper-Zubillaga et al., 2008; Rao et al., 2011). Geochemical methods are useful tools for identifying sand transport and its sources, because some geochemical signature can reflect transport processes on the one hand, while on the other hand some maintain invariant ratios during post-depositional chemical weathering. For instance, the major elements and rare earth elements (REE) of sand sediments in desert fluvial systems can record both wind and fluvial transport process (Yang et al., 2007a). The REE spatial distribution are also useful to determine the relative mobility of sands (Kasper-Zubillaga et al., 2008) and Ce negative anomalies represent an useful index for interpreting the histories of sedimentary environments (Liu and Yang, 2013). In more recent years, attention has also been given to the fluvial processes while investigating the formation and changes of desert sand seas (Al-Janabi et al., 1988; Wopfner and Twidale, 1988; Yang et al., 2011). Either a river system can or cannot stop the migration of dune fields can also be recorded as some geochemical signature (Muhs et al., 2000, 2003). Some major elements are useful indicators to separate sands derived from aeolian processes from those derived from fluvial processes (Zimelman and Williams, 2002). Trace elements or immobile elements, combined with other evidence, are good indicators for the orientations of paleowinds (Arbogast and Muhs, 2000), as well as good indicators for ancient aeolian activity in dune field (Muhs et al., 1997).

The primary objectives of this work, on the basis of geochemical studies of aeolian sands surrounding the Minqin Oasis, are to recognize the spatial variation of sand sources around the oasis, and

to identify the transport pathways of the sandy sediments in the arid region.

## 2. Regional setting

For this study, samples were collected from the Minqin Oasis and the margins of other two large sand seas, i.e., the Badain Jaran Desert (the 2nd largest sand sea in China) and Tengger Desert (the 3rd largest sand sea in China) which border the Minqin Oasis to the northwest and the southeast, respectively (Fig. 1). With an area of  $\sim 1500 \text{ km}^2$ , the Minqin Oasis is located in the western part of the Gansu Province, northwestern China. It is characterized by a markedly arid climate with a mean annual precipitation of 113 mm, and a mean annual temperature of  $8.3 \text{ }^\circ\text{C}$  (data from China Meteorological Data Sharing Service System). The water supply of the Minqin Oasis is mainly from the Shiyanghe River, whose supply is from atmospheric precipitation and the melting of glaciers in the Qilian Mountains. It has a catchment area of  $41.6 \times 10^3 \text{ km}^2$  and its annual total surface runoff is  $1.58 \times 10^9 \text{ m}^3$  via eight tributaries (Ma et al., 2005). From west to east these comprise the Xidahe River, Dongdahe River, Xiyinghe River, Jintahe River, Zamuhe River, Huangyanghe River, Gulanghe River, and Dajinghe River (Fig. 1). The river system crosses three climatological zones: i) the headwaters in the cold and humid to semi-arid Qilian Mountains zone are located between 2000 and 5000 m above sea level (m a.s.l.) with mean annual precipitation varying markedly from 300 to 600 mm; ii) the midstream temperate zone is located between 1400 and 2000 m a.s.l. in the Wuwei Basin with a mean annual precipitation of 150–300 mm, and iii) the downstream warm temperate zone, 1000–1400 m a.s.l. in the Minqin Basin (Tang et al., 1992).

With an area of  $\sim 49,200 \text{ km}^2$ , the Badain Jaran Desert stands on the Alashan Plateau where small mountains consisting of igneous rocks occur occasionally (Ma, 2002). Desert plains, gravel deserts (Gobi) and palaeochannels surround the desert. The Badain Jaran is particularly characterized by the occurrence of tall dunes, some of which stand higher than 400 m, and large permanent lakes occur in the inter-dune depressions (Yang et al., 2010). The mean annual precipitation decreases from  $\sim 120 \text{ mm}$  in the southeast to  $\sim 40 \text{ mm}$  in the northwestern of the desert, with a mean annual evaporation rate of  $\sim 1000 \text{ mm}$  from the lake surface and  $\sim 100 \text{ mm}$  from the land surface in the southeastern part of the sand sea (Yang et al., 2010). With an area of ca.  $42,700 \text{ km}^2$ , the Tengger Desert is located in the southeast of the Minqin Oasis. Two thirds of this sand sea is occupied by dunes, 93% of which are active, while vegetated lake beds, dry salt lakes, and basement hills are common in the remaining area of this sand sea. The main types of dunes are net-shaped ones in the interior part of this sand sea, and long dune chains on the margins. Under the prevailing winds from the northwest, the dunes tend to move southeastwards (Zhu et al., 1980; Yang et al., 2004, 2012).

## 3. Methods

Sandy sediments samples were collected from the areas of the oasis and its surrounding deserts. As the small active dunes migrate faster than the large ones, we targeted dunes lower than 10 m in height for sampling. A total of 76 sand samples were taken from six different sub-regions: 20 bulk samples along an 80 km transect from SW to NE at the southeastern margin of the Badain Jaran Desert (B), 21 bulk samples from dune belt connecting the Badain Jaran Desert and the Minqin Oasis (BM), 6 bulk samples from the Minqin Oasis area (M), 29 bulk samples from the NW margin of the Tengger Desert including 12 samples to the northeast of the oasis

(TNE), 6 samples to the southeast of the oasis (TM) and 11 samples to the south of the oasis (TSW) (Fig. 1).

Wind records covering the period from 2001 to 2011 from the six meteorological stations at the periphery of the study area were used to interpret the potential movement of sand. Sand drift potential (DP), resultant drift potential (RDP), the directional variability (RDP/DP) and the resultant direction of sand movement (RDD) were estimated following Fryberger and Dean (1979, Table 1). The wind data are from China Meteorological Data Sharing Service System.

**Table 1**

Sand drift potential (DP), resultant drift potential (RDP), the resultant direction of sand movement (RDD, 0 referring to the north, clockwise) and the directional variability (RDP/DP) based on wind records at the margins of the study area from 2001 to 2011 (vector units with wind speed in knots).

	Alashan right banner	Bayinmaodao	Minqin	Wuwei	Yongchang	Zhongwei
DP	230.77	462.67	92.48	29.73	119.46	82.76
RDP	75.83	295.09	75.55	24.92	111.08	41.52
RDP/DP	0.33	0.64	0.82	0.84	0.93	0.50
RDD	310.72	123.06	120.23	130.04	115.92	127.21

Bulk samples were taken for laboratory preparation and measurements in the Key Laboratory of Western China's Environmental System, Lanzhou University. All samples were dried at low temperature ( $43 \text{ }^\circ\text{C}$ ) for 72 h and grinded to less than  $75 \text{ }\mu\text{m}$ . Up to 4 g of sample was weighed and poured into the center of the column apparatus, together with boric acid, and pressurized to  $30 \text{ t/m}^2$  for 20 s using a YYJ-40 semiautomatic oil hydraulic apparatus. The processed samples, approximately 4 cm in diameter and 8 mm thick, were analyzed by using a Philips Panalytical Magix PW2403 X-ray fluorescence (XRF) spectroscope. Analytical results are reported in oxide compound form apart from trace elements which are given in elemental form. The standard deviations for the major elements were estimated by the repeated analysis of the samples. Standard deviations were  $<10\%$  for Ce, Co, Cs, Ga, La, Rb, Sc, Y, Hf and Zr,  $<8\%$  for Ba, Bi, Cr, Mn, Ni, Sr and V,  $<3\%$  for MgO and Na<sub>2</sub>O and  $<0.5\%$  for the other major elements. The chemical index of alteration (CIA) was calculated using the formula proposed by Nesbitt and Young (1982), i.e.  $\text{CIA} = [\text{Al}_2\text{O}_3 / (\text{Al}_2\text{O}_3 + \text{CaO}^* + \text{Na}_2\text{O} + \text{K}_2\text{O})] \times 100$  (ratio in molecular proportions). Here CaO\* refers to the amount of CaO only incorporated in the silicate fraction and is calculated using  $\text{CaO}^* = 0.35 \times 2\text{Na}_2\text{O}$  (in weight %)/62 (Honda and Shimizu, 1998).

Our analysis of geochemical data focuses on element abundance and element ratio methods widely used in geochemistry (Sun, 2002; Yang et al., 2007a, 2007b; Ujvari et al., 2008; Buggle et al., 2011; Qiao et al., 2011). In addition we apply hierarchical cluster analysis of the data to group samples on the basis of multi-elements analysis (Bridges, 1966; Johnson, 1967; D'Andrade, 1978). Hierarchical cluster analysis, based on Ward's method (Ward, 1963) and the Euclidean distance, was conducted to classify samples using trace elements as the variables (Wolff and Parsons, 1983). To simplify the analyses, the geochemical data for sub-region B represent the average element abundance of 20 samples in the Badain Jaran Desert, while the average element abundance of 21 samples was used for the BM region. Trace elements (Ba, Bi, Ce, Co, Cr, Cs, Ga, La, Mn, Rb, Sr, V and Zr) and Ti whose average abundance were larger than 20 ppm were selected for hierarchical cluster analysis in order to avoid errors caused by the detection limit of our instrument. To reduce the impact of the large difference in abundance level of the various elements, the data were standardized to z scores, with a mean of 0 and a standard deviation of 1 (Templ et al.,



2008; Xue et al., 2011). Hierarchical cluster analysis was performed using the IBM SPSS Statistics 20 program.

4. Results

In general, the aeolian sands from different sub-regions of the study area (B, BM, TNE, TM, TSW and M) show different abundances of major and trace elements (Fig. 1 and Table 2). The contents of SiO<sub>2</sub> are very high and range from 72.2% to 88.9% with a mean value of 83.3%. In contrast, most of the trace elements are relatively low, only Ba, Ce, Co, Mn, Sr reach a content >100 ppm. In each sub-region, Ba, SiO<sub>2</sub>, Rb, Sr, Al<sub>2</sub>O<sub>3</sub> and K<sub>2</sub>O are relatively homogeneous by comparison with the average composition of the upper continental crust (UCC, Taylor and McLennan, 1985), whereas other elements are variable with some clear heaves and depressions (Fig. 2). In terms of major elements, only SiO<sub>2</sub> is enriched relative to UCC, while for trace elements, the majority of them are depleted

except Cr and Ni that are enriched in the sub-regions B and BM as well as Cr enriched in TNE.

Here, we used K, Rb, Sr and Ba to trace spatial variations of mobile elements and further to identify the transport pathways of the aeolian sediments. These four elements are low field strength (LFS) elements which are likely to become mobilized when any suite of rocks is subjected to hydrothermal alteration or metamorphism (Rollinson, 1993). Referring to the contents of the LFS elements (Fig. 3), the sediments from the sub-regions B, BM and TNE are similar and distribute linearly, with sub-region B falling into the lower fields of the linear regression lines. In addition, the sediments in the TM sub-region are different from those of the other five sub-regions, while the sediments in TSW and M sub-regions are in the same group. Furthermore, the values of the ratios K/Rb, Ba/Rb and Sr/Rb of sub-regions B (mean 207.10, 7.75 and 2.19, respectively), BM (mean 207.37, 7.56 and 2.02, respectively) and TNE (mean 201.25, 7.75 and 2.01, respectively) are, overall, significantly higher than those in TSW (mean 170.86, 5.56 and 1.60,

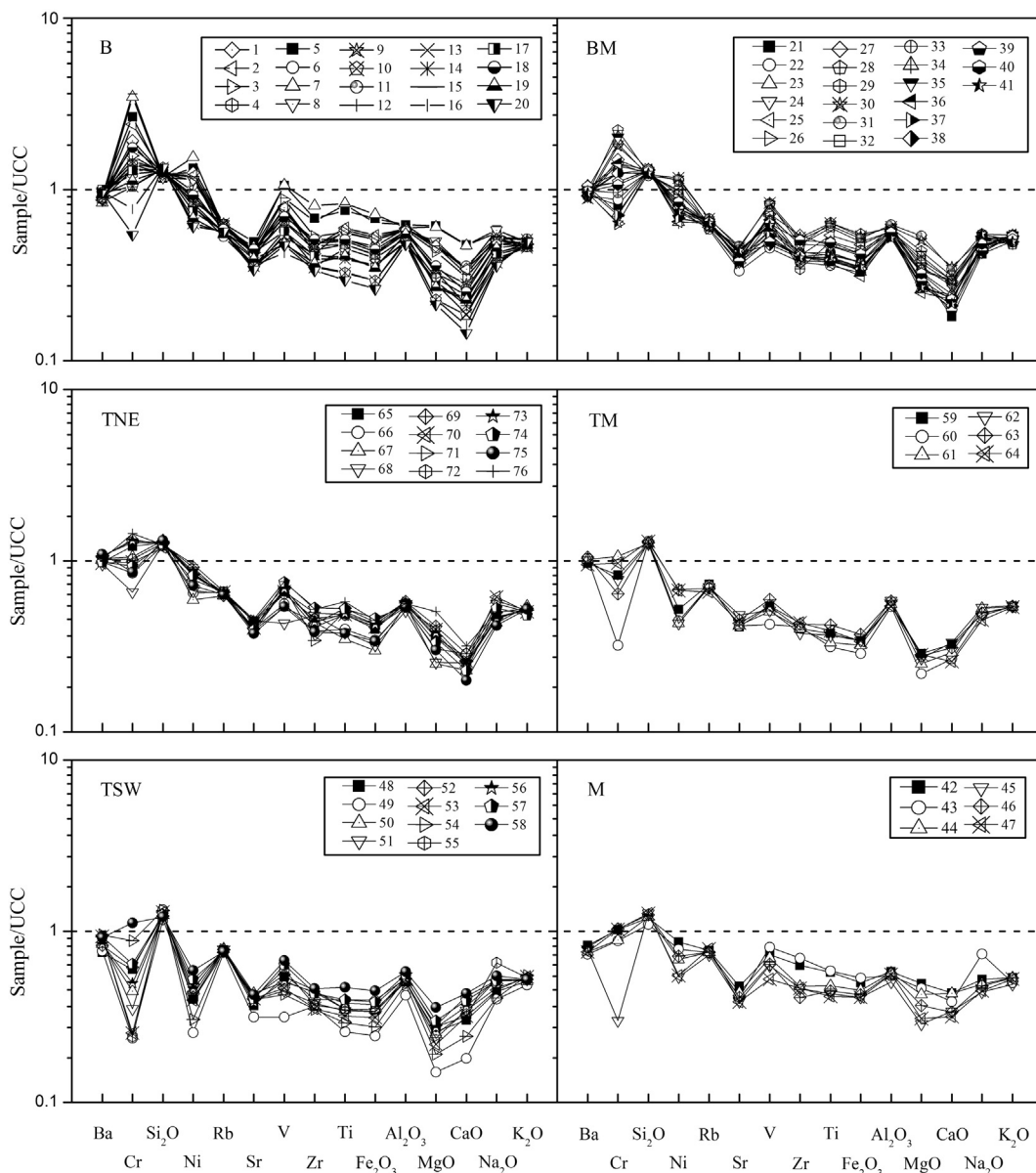


Fig. 2. Elemental enrichment plots in the six sub-regions (as divided in Fig. 1). The elements are shown as enrichments normalized to upper continental crust (UCC).

**Table 2**  
Abundance of major (%) and trace elements (ppm) in the sand samples.

	B																				M							BM												
	1	2	3	4	5	6	7	8	9	10	11	12	13	14	15	16	17	18	19	20	42	43	44	45	46	47	21	22	23	24	25	26	27	28	29	30	31	32	33	
<b>%wi</b>																																								
TFe <sub>2</sub> O <sub>3</sub>	3.04	2.09	3.23	2.29	2.36	2.43	2.30	1.88	1.86	1.32	1.79	1.63	1.62	1.95	2.88	1.32	1.58	2.01	1.57	1.18	2.25	2.40	2.03	1.85	1.91	1.85	1.70	1.47	1.69	1.90	2.14	1.54	1.85	2.47	1.99	2.40	2.33	2.22	1.68	
SiO <sub>2</sub>	77.0	80.9	77.8	78.1	81.4	81.6	82.2	84.7	82.4	88.6	86.2	87.1	86.9	85.7	80.8	88.9	86.5	83.6	85.7	88.9	79.0	72.2	80.0	84.2	82.2	83.8	85.6	84.7	84.5	83.4	81.7	85.4	83.1	81.8	82.5	80.8	79.3	81.1	83.5	
Al <sub>2</sub> O <sub>3</sub>	9.47	9.01	9.09	8.73	8.94	8.99	8.82	8.84	8.45	7.55	7.89	7.58	7.49	8.47	9.48	7.73	8.36	8.69	8.38	7.29	8.81	8.34	8.65	7.66	8.56	8.50	7.99	8.06	8.82	9.15	8.72	8.20	8.91	9.08	8.59	9.19	9.47	8.68	8.47	
MgO	1.35	1.00	1.33	1.10	1.03	1.06	0.96	0.71	0.76	0.50	0.67	0.64	0.62	0.74	1.03	0.50	0.60	0.79	0.59	0.47	1.09	1.02	0.94	0.63	0.81	0.68	0.72	0.61	0.72	0.78	0.85	0.60	0.74	0.96	0.82	1.11	1.18	0.90	0.75	
CaO	1.99	1.50	1.98	1.44	1.44	1.44	1.29	1.11	1.18	0.78	1.01	0.88	0.79	0.88	1.35	0.68	0.97	1.06	0.95	0.61	1.83	1.63	1.82	1.43	1.41	1.33	0.76	0.85	1.03	1.15	1.24	0.97	1.22	1.31	1.19	1.48	1.44	1.23	1.24	
Na <sub>2</sub> O	2.26	2.06	2.18	2.26	1.99	1.96	1.95	1.87	2.02	1.46	1.63	1.50	1.55	1.68	2.06	1.42	1.65	1.86	1.78	1.40	2.04	2.87	1.91	1.72	1.87	1.75	1.64	1.86	1.84	1.96	2.08	1.83	2.00	2.02	1.99	2.02	2.14	2.12	1.92	
K <sub>2</sub> O	1.67	1.75	1.55	1.68	1.64	1.64	1.63	1.68	1.73	1.65	1.57	1.60	1.55	1.59	1.54	1.66	1.65	1.62	1.63	1.69	1.82	1.70	1.82	1.66	1.81	1.79	1.70	1.70	1.83	1.82	1.68	1.68	1.79	1.63	1.68	1.80	1.84	1.74	1.79	
TiO <sub>2</sub>	0.38	0.25	0.42	0.28	0.29	0.30	0.28	0.24	0.24	0.16	0.23	0.20	0.20	0.25	0.41	0.16	0.20	0.26	0.20	0.15	0.29	0.29	0.24	0.22	0.22	0.21	0.21	0.18	0.21	0.24	0.27	0.19	0.23	0.32	0.25	0.32	0.31	0.30	0.21	
Total	97	99	98	95.8	99	99	99	101	99	102	101	101	101	101	100	102	102	100	101	102	97.1	90.4	97.4	99	99	100	100	99	101	100	99	100	100	99	99	98	98	98	100	
CIA(%)	53.8	54.0	53.9	51.7	54.9	55.3	55.0	55.6	52.9	56.2	55.8	56.1	55.5	56.9	56.1	57.2	56.6	55.5	55.4	55.9	53.4	45.8	54.2	53.7	54.3	55.4	55.4	53.4	55.3	55.1	53.3	54.2	54.2	55.0	53.8	54.7	54.3	52.6	53.7	
<b>ppm</b>																																								
Ba	520	511	461	481	493	477	500	534	515	527	484	465	494	530	497	536	550	530	515	533	454	403	416	430	443	417	514	505	556	552	507	526	502	520	520	488	510	527	544	
Bi	20.4	21.9	17.4	20.1	20.1	21.0	18.5	21.0	22.1	21.9	22.4	22.2	16.1	24.5	20.7	18.8	17.8	19.3	18.4	22.6	20.1	17.1	18.0	22.7	22.3	20.3	20.3	20.8	18.6	16.2	21.8	17.3	19.7	17.6	16.6	18.4	19.4	19.2	22.0	
Ce	108	88.2	167	113	103	104	151	103	107	92.6	101	89.3	88.0	102	106	91.1	85.8	100	128	124	163	192	122	173	124	151	111	137	62.1	82.8	129	113	125	121	96.5	136	112	109	82.5	
Co	136	141	300	140	184	176	246	248	183	258	263	225	223	266	193	285	237	207	263	265	208	164	140	410	194	281	229	238	195	199	197	257	188	239	251	257	150	211	237	
Cr	93.1	49.4	122	64.4	67.6	84.2	55.2	43.2	46.5	36.4	45.8	36.4	49.5	51.5	127	26.9	45.1	61.5	39.4	19.1	35.7	30.8	31.1	10.5	36.1	35.9	28.3	30.6	38.9	48.1	49.4	22.1	52.5	77.7	43.6	62.8	64.7	44.1	33.5	
Cs	24.9	30.7	23.4	25.7	31.0	28.0	26.3	29.7	30.5	36.5	35.9	38.6	25.9	38.2	27.0	31.4	27.7	26.3	28.8	34.6	25.8	18.6	25.4	37.8	30.7	31.8	31.5	31.0	28.0	22.6	30.4	27.1	28.8	24.2	23.0	23.7	26.6	27.1	32.6	
Ga	25.4	22.6	25.0	25.5	24.1	25.3	25.0	25.1	24.2	24.8	24.6	23.3	24.2	24.1	24.6	23.2	24.8	25.4	23.9	23.8	25.6	24.7	23.3	24.6	26.1	24.5	24.9	24.9	24.2	25.8	25.9	24.6	24.0	24.2	26.3	25.0	25.6	24.5	24.5	
Hf	3.5	2.5	4.2	2.4	2.1	2.3	2.6	2.1	2.3	1.5	1.6	1.8	1.9	2.3	3.4	1.5	1.9	2.5	1.7	1.4	3.5	4.0	2.6	2.4	2.2	2.4	1.9	1.7	2.0	2.3	2.0	1.7	2.7	2.3	1.6	2.7	2.6	2.3	2.0	
La	21.7	1.9	34.5	23.8	14.7	25.1	10.9	15.9	32.3	15.8	29.8	12.3	15.0	32.6	28.7	4.2	29.9	25.9	27.5	20.9	46.8	31.3	21.5	22.4	24.8	33.0	32.4	20.3	15.2	22.3	39.3	33.6	8.4	17.2	10.9	25.3	32.4	24.0	34.9	
Mn	416	304	436	317	329	335	314	260	245	173	234	212	199	243	370	173	204	249	199	156	280	275	268	246	248	239	213	192	233	261	288	214	259	331	280	314	304	292	216	
Ni	26.7	18.2	31.0	22.8	25.1	24.1	22.5	17.7	17.1	12.7	16.0	15.9	16.6	19.5	23.8	12.3	14.9	18.5	13.6	12.2	17.3	15.7	13.7	10.8	14.3	11.0	17.0	15.3	16.4	16.9	19.4	14.8	16.2	22.5	18.8	23.4	22.9	19.8	15.6	
Rb	70.7	69.1	67.9	70.6	70.0	67.9	67.5	71.0	63.1	59.4	62.6	62.9	64.1	60.8	63.6	63.7	65.7	61.3	63.9	86.5	84.1	84.3	81.6	84.4	88.2	66.9	65.7	71.7	72.1	67.6	66.4	71.2	68.5	70.8	75.6	75.5	71.4	69.2		
Sc	9.7	6.9	9.6	8.5	7.1	8.8	7.4	6.4	7.0	5.7	6.3	5.2	6.4	5.9	8.4	5.1	5.8	6.5	5.5	4.9	7.4	7.7	6.4	5.5	6.6	6.1	5.5	5.8	5.4	6.8	7.4	5.2	6.3	8.1	5.6	7.0	7.1	6.8	6.4	
Sr	174	153	161	154	155	147	150	152	146	125	124	119	125	140	160	127	150	157	138	120	166	144	153	136	144	135	126	117	140	137	144	131	136	161	151	160	164	139	155	
V	63.5	44.1	63.9	46.2	47.1	47.4	52.5	39.0	39.2	29.4	34.7	33.1	31.8	42.7	53.5	25.6	34.2	41.7	28.9	28.4	43.9	48.3	41.9	37.8	38.4	31.5	30.5	27.3	34.7	41.5	42.2	32.9	43.2	49.8	39.3	50.1	49.0	42.2	37.6	
Y	17.5	13.5	18.6	15.1	15.9	15.0	15.1	12.6	13.3	11.0	11.3	11.4	11.4	12.7	19.0	9.9	12.1	15.9	11.1	10.8	16.9	17.5	17.1	14.2	15.3	14.9	11.8	11.5	13.2	12.9	14.0	11.2	13.6	14.9	12.7	15.8	15.1	14.9	11.2	
Zr	129	94.6	153	90.2	80.3	87.9	101	84.1	89.1	66.7	67.4	74.5	79.1	91.9	124	67.5	77.8	97.5	70.4	64.1	120	132	90.4	88.1	77.8	88.2	77.3	71.5	81.9	91.1	78.2	72.7	103	90.4	65.3	99.8	96.7	90.2	81.2	
<b>%wt</b>																																								
TFe <sub>2</sub> O <sub>3</sub>	1.49	1.51	1.41	1.57	1.55	1.52	1.89	1.59	1.57	1.10	1.57	1.52	1.78	1.41	1.24	1.53	1.68	1.74	2.02	1.53	1.29	1.44	1.53	1.67	1.52	1.79	1.54	1.34	1.44	1.97	1.84	1.92	1.85	1.90	2.07	1.52	2.01			
SiO <sub>2</sub>	86.0	85.1	86.0	86.3	86.4	85.9	84.4	82.1	84.6	87.9	82.1	83.7	81.0	85.4	87.4	77.2	81.7	82.5	80.1	83.6	85.3	83.2	82.7	84.2	85.5	84.0	80.5	86.4	82.1	82.6	78.5	84.2	83.9	84.1	82.4	86.5	81.7			
Al <sub>2</sub> O <sub>3</sub>	8.49	8.43	8.32	8.44	8.35	8.35	7.89	7.69	6.41	7.79	7.68	8.02	7.97	7.44	8.09	8.17	8.52	8.81	8.40	8.18	8.46	8.87	8.82	8.27	8.55	8.11	8.42	7.71	8.75	8.16	8.60	8.52	8.67	8.20	8.18	8.55				
MgO	0.58	0.65	0.55	0.59	0.63	0.64	0.71	0.59	0.57	0.33	0.55	0.52	0.62	0.48	0.42	0.61	0.60	0.66	0.79	0.63	0.48	0.55	0.59	0.61	0.62	0.78	0.67	0.55	0.56	0.91	0.87	0.80	0.78	0.83	0.73	0.66	1.11			
CaO	1.02	0.95	0.96	0.98	0.88	0.82	0.96	0.90	1.27	0.76	1.43	1.45	1.75	1.34	1.02	1.34	1.53	1.65	1.82	1.36	1.12	1.22	1.40	1.30	1.08	1.15	1.20	0.96	1.06	1.20	1.09	1.08	1.05	1.04	0.96	0.84	1.33			
Na <sub>2</sub> O	1.79	1.80	1.79	1.72	1.67	1.71	1.88	2.15	1.73	1.56	2.04	1.82	2.01	1.77	1.59	2.55	2.04	2.00	2.14	1.92	1.86	2.05	2.07	1.93	1.75	1.83	2.27	1.69	2.18	1.94	2.39	1.80	1.80	1.78	2.06	1.63	1.96			
K <sub>2</sub> O	1.83	1.85	1.84	1.82	1.83	1.82	1.75	1.69	1.74	1.65	1.73	1.81	1.78	1.84	1.87	1.82	1.77	1.76	1.77	1.83	1.8																			

Table 2 (continued)

	TSW										TM										TNE																
	34	35	36	37	38	39	40	41	48	49	50	51	52	53	54	55	56	57	58	59	60	61	62	63	64	65	66	67	68	69	70	71	72	73	74	75	76
La	21.0	25.7	14.9	3.8	33.3	27.1	40.5	33.9	7.5	25.3	17.6	19.7	11.9	25.9	21.7	24.2	37.4	33.7	26.0	47.9	29.4	26.1	33.4	40.6	28.0	27.4	31.6	30.4	10.9	21.8	37.8	35.5	11.9	6.7	30.7	15.8	4.6
Mn	220	213	208	224	213	211	250	216	221	165	231	233	272	219	183	223	254	257	281	216	188	195	219	251	211	224	202	174	188	232	205	226	217	227	237	182	229
Nb	5.5	5.7	5.0	4.8	6.1	4.9	5.9	5.1	5.8	4.1	5.4	4.9	5.6	3.9	4.3	4.8	6.0	5.7	7.3	5.3	4.3	4.7	5.0	5.9	6.0	7.3	6.4	5.5	5.8	6.2	6.7	6.8	6.3	6.9	6.8	4.7	7.4
Ni	12.9	13.5	13.0	13.6	15.5	15.4	16.9	14.8	8.0	5.1	9.1	8.5	9.8	7.9	6.1	8.1	9.2	10.5	11.8	10.4	8.9	8.6	8.6	13.5	13.4	16.9	12.9	11.8	13.3	18.3	15.5	16.6	16.3	17.3	16.4	14.3	19.0
Rb	71.5	72.2	70.7	70.1	72.9	72.1	72.0	71.4	87.4	83.9	88.1	87.7	87.5	84.2	87.4	86.4	86.9	84.5	85.1	81.3	79.8	79.4	78.4	77.4	73.2	71.1	73.3	69.8	72.0	70.0	73.2	73.3	73.5	73.0	71.2	71.0	74.1
Sc	5.3	6.3	5.7	5.4	5.6	6.4	5.9	5.2	6.0	5.3	4.4	5.8	5.5	5.9	4.6	6.3	6.4	5.9	7.4	6.6	5.5	6.5	6.5	5.5	5.5	5.5	7.1	5.8	5.3	5.5	5.9	7.0	6.7	6.0	6.0	4.5	6.9
Sr	147	133	136	136	148	133	151	154	128	110	152	139	145	142	139	144	135	141	149	144	145	147	169	158	151	156	140	137	156	140	142	156	153	134	138	131	159
V	31.1	38.4	34.4	32.0	28.6	29.7	37.9	37.0	32.6	18.9	30.3	27.0	33.5	27.9	25.6	35.7	30.7	38.3	40.4	32.5	25.5	30.3	30.7	35.5	32.6	39.5	33.5	32.0	25.8	41.2	39.5	42.1	38.2	41.0	44.9	32.3	45.3
Y	11.8	12.3	11.0	11.1	11.2	12.4	13.4	11.6	14.6	11.2	13.2	13.7	14.6	11.4	10.9	13.0	14.2	14.3	15.4	13.5	11.0	12.1	12.3	13.3	12.2	13.4	13.2	11.7	11.6	13.4	14.8	13.5	13.6	14.3	14.5	11.3	15.0
Zr	77.1	77.6	77.8	77.1	75.9	77.4	96.2	75.8	85.9	69.4	83.5	72.1	76.1	67.1	66.3	70.4	83.1	82.2	87.9	76.0	77.8	76.1	71.6	81.0	82.4	77.7	73.5	82.8	90.8	81.6	94.1	65.0	87.2	83.1	101	72.8	98.8

respectively) and M (mean 172.77, 5.04 and 1.73, respectively). These ratios have medium values in TM (mean 194.79, 7.04 and 1.95, respectively). In contrast, the K/Ba values of sub-regions B (mean 26.78), BM (mean 27.47), TNE (mean 26.00) and TM (mean 27.69) are lower than in TSW (mean 30.89) and M (mean 34.35).

By contrast with LFS elements, plots referring to relatively immobile elements show linear distributions in all sub-regions. In plots of Cr vs. Ni, Ni vs. Al, Cr vs. Al, V vs. Ni and V vs. Cr (Fig. 4a, c, d, e and f), the correlation coefficients  $R^2$ , are 0.71, 0.47, 0.45, 0.71 and 0.58 respectively. Although abundances of these elements show a wide range of variability, TSW is inclined to appear in the lower part of the linear regression lines in each plots, indicating relatively lower content of Ni, Cr, V and Al than those in sub-regions B, BM and TNE. The plot of Cr/V and Y/Ni (Fig. 4b) shows that samples in B (range of 0.67–2.37 for Cr/V and 0.60–0.89 for Y/Ni), BM (range of 0.61–1.84 for Cr/V and 0.66–0.91 for Y/Ni) and TNE (range of 0.72–1.15 for Cr/V and 0.73–1.02 for Y/Ni) overlap and concentrate at the high end member whereas samples in TSW (range of 0.24–1.20 for Cr/V and 1.31–2.20 for Y/Ni) overlap less and are scattered in the low end member, while TM samples with ranges of 0.44–1.22 for Cr/V and 0.91–1.43 for Y/Ni as well as M samples with range of 0.28–1.14 for Cr/V and 0.98–1.35 for Y/Ni, are plotted in the area between them.

High field strength elements (HFS) Zr and Hf were chosen for comparison of sandy sediments in the six sub-regions. When plotted together, the 76 samples in all sub-regions show a clear linear distribution and very high correlation (Fig. 5a), reconfirming that the data are reliable. The plot of Zr/Hf vs. Hf shows that two exponential regression curves can be fitted through the data points, one for the B, BM and TNE samples ( $n = 53$ ) and the other for the TSW samples ( $n = 11$ ). The TM and M samples fall in the areas between these two curves (Fig. 5b).

Regional variations of the sediments can also be recognized in the ternary plots of various trace and major element compositions. In ternary plots of Rb, Sr and Ba (Fig. 6a), all the six sub-regions are characterized by abundant Ba with much smaller amounts of Sr and Rb. However, TSW have relatively higher Rb than B, BM and TNE sub-regions do. In ternary plots of Y, Sc and Ce (Fig. 6b), abundances of Y and Sc are generally lower while Ce is higher in TSW than in the regions of B, BM and TNE. Samples from TM and M fall in between these two groups. Major elements also show similar spatial distribution. For instance, Figs. 7 and 8 show that proportions of  $\text{TFe}_2\text{O}_3$ ,  $\text{K}_2\text{O}$ ,  $\text{Na}_2\text{O}$  are similar in all six sub-regions. In contrast, proportions for  $\text{Al}_2\text{O}_3$ , MgO and CaO are more variable. TSW samples have, on average, lower  $\text{Al}_2\text{O}_3$  and MgO and higher CaO than B, BM and TNE samples. TM and M samples overlap these two groups. These differences, however, are not obvious and there is considerable overlap in the plots for  $\text{TFe}_2\text{O}_3 + \text{MgO}$ ,  $0.1\text{SiO}_2$  and  $\text{Na}_2\text{O}$  (Fig. 9a) and plots for  $\text{TFe}_2\text{O}_3$ ,  $0.5\text{SiO}_2$  and CaO (Fig. 9b).

In plots of A–CN–K (Fig. 10), samples in TSW except for one samples, concentrate into a narrow area of the plot and are characterized by relatively low abundance of  $\text{Al}_2\text{O}_3$  and relatively high  $\text{CaO}^* + \text{Na}_2\text{O}$  compared with B, BM and TNE samples. TM and M samples fall into an intermediate area between these two groups. The values of CIA are similar in all sub-regions ranging from 45 to 58. On average, CIA values in TSW, M and TM are relatively lower than those in B, BM and TNE.

## 5. Discussion

### 5.1. Differentiation of sand sources in northwest and southeast sides of the oasis

The sand samples of the sub-regions B, BM and TNE (in the west and north sides of the oasis) are chemically different from

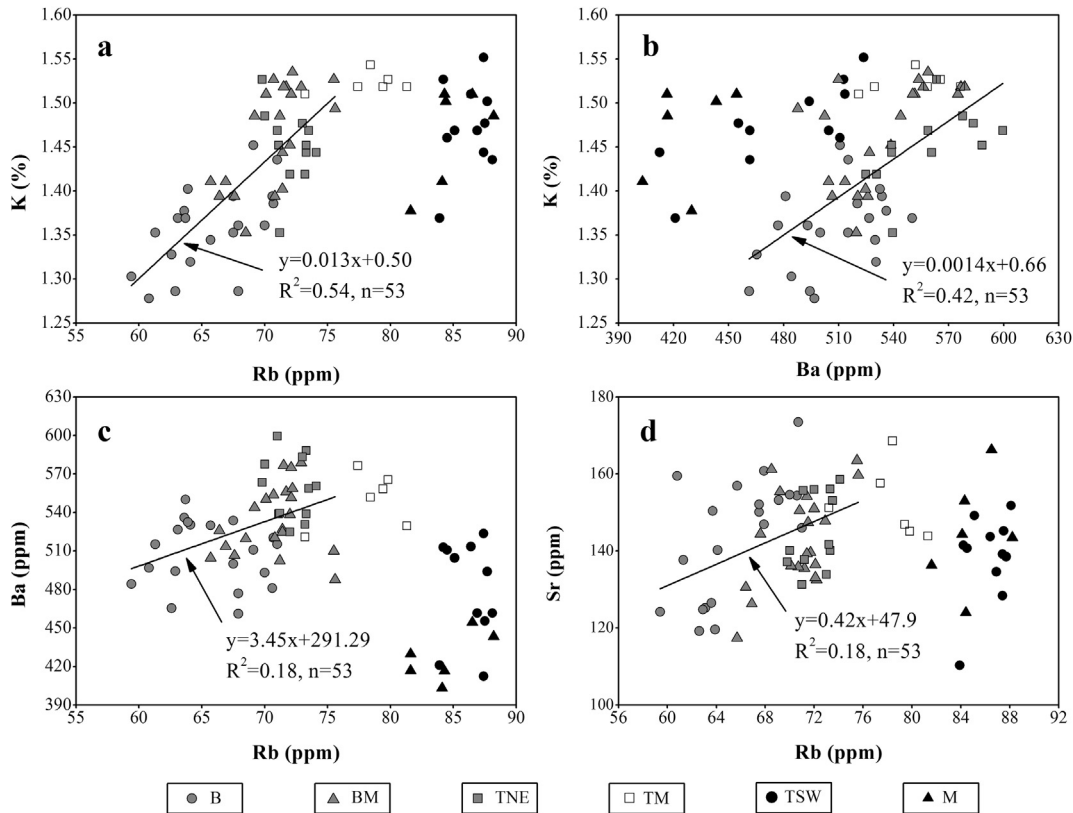


Fig. 3. Bivariate plots of low field strength (LFS) elements. (a) K vs. Rb, (b) K vs. Ba, (c) Ba vs. Rb and (d) Sr vs. Rb.

those of TSW (in the southeast side of the oasis), as confirmed by the geochemical immobile elements V, Cr and Ni as well as element ratios associated with them. For instance, the plots of Ni vs. Al and Cr vs. Al (Fig. 4c and d) show that sub-regions B, BM and TNE are characterized by higher average Ni, Cr and Al compared with sub-region TSW. This difference in spatial distribution is also apparent in the Cr vs. Ni, V vs. Ni, and V vs. Cr plots (Fig. 4a, e and f). These elements are thought to be suitable for the determination of the provenance because of their relatively low mobility during sedimentary processes (Rollinson, 1993). More importantly, it was found that the ratios Ni/Al and Cr/Al are not obscured or affected by grain size variations (Dinelli et al., 2007), and therefore, are very suitable for the analysis of bulk samples as done in our study.

The Cr/V and Y/Ni ratios (Fig. 4b) also illustrate the various degree of contribution of felsic and mafic sources to these two groups of samples. The Cr/V ratio is an index of the enrichment for Cr relative to other ferromagnesian trace elements, whereas Y/Ni is a measure for the general level of ferromagnesian trace elements (Ni) compared to Y which is a proxy for heavy REE (McLennan et al., 1993). Mafic and ultramafic source rocks tend to have high Cr/V and low Y/Ni ratios, on the contrary, felsic rocks have low Cr/V and high Y/Ni (McLennan et al., 1993). When we apply the McLennan' plot for Cr/V vs. Y/Ni (McLennan et al., 1993) to our data, samples of B, BM and TNE show high Cr/V and low Y/Ni ratios, suggesting mafic and ultramafic sources. In contrast, TSW samples have low Cr/V and high Y/Ni ratios, suggesting a greater contribution of felsic rocks. Furthermore, the values normalized to UCC for Cr and Ni, are higher in B, BM and TNE than in TSW (Fig. 2). This suggests more Cr-bearing and Ni-bearing minerals in B, BM and TNE than in TSW, which confirm that the contributions from mafic and felsic sources are different between these two groups of samples.

The content of the HFS elements Zr and Hf are also different between these two groups. The Zr/Hf values in sub-regions of B (mean 40.05), BM (mean 40.50) and TNE (mean 40.64) are higher than in the sub-region of TSW (mean 37.99). These differences are more distinct in the plot of Zr/Hf vs. Hf (Fig. 5b) that shows two different exponential distributions. This kind of exponential distribution pattern is also found in granitic zircons (Wang et al., 2010; Canosa et al., 2012). Zr and Hf are considered relatively immobile and do not fractionate appreciably during weathering (Taylor and McLennan, 1985). They are normally enriched in zircon, one of the ultra-stable minerals frequently used in sediment source discrimination. Thus, Zr/Hf at least partly reflects the compositional changes of zircon. Hence, the different contents of Zr and Hf in these two groups are most likely to be caused by sandy sediments which are associated with different heavy mineral enrichments (i.e. zircon enrichments).

Major elements could also be good indices for sand provenance. Zimelman and Williams (2002) successfully explored the discrimination potential of major oxide chemistry for bulk aeolian sand samples. Similarly, in our study, major element proportions in B, BM and TNE are chemically different from those of TSW in ternary plots (Figs. 7 and 8), although these differences are not obvious in the plots of SiO<sub>2</sub>, Na<sub>2</sub>O and Fe<sub>2</sub>O<sub>3</sub> + MgO (Fig. 9). This could be due to the significant dilution by SiO<sub>2</sub>. In our samples, the content of SiO<sub>2</sub> is very high, higher than in the samples from the Taklamakan Desert (with a mean value of 60.2%, Zhu and Yang, 2009), the biggest sandy desert in China (Zhu et al., 1980). Therefore, the major elements without SiO<sub>2</sub> should better reflect the chemical differences between these two groups. In addition, chemical difference may be caused by different intensity of chemical weathering as it controls the fractionation of major elements. However, all samples in this study have similar CIA values,

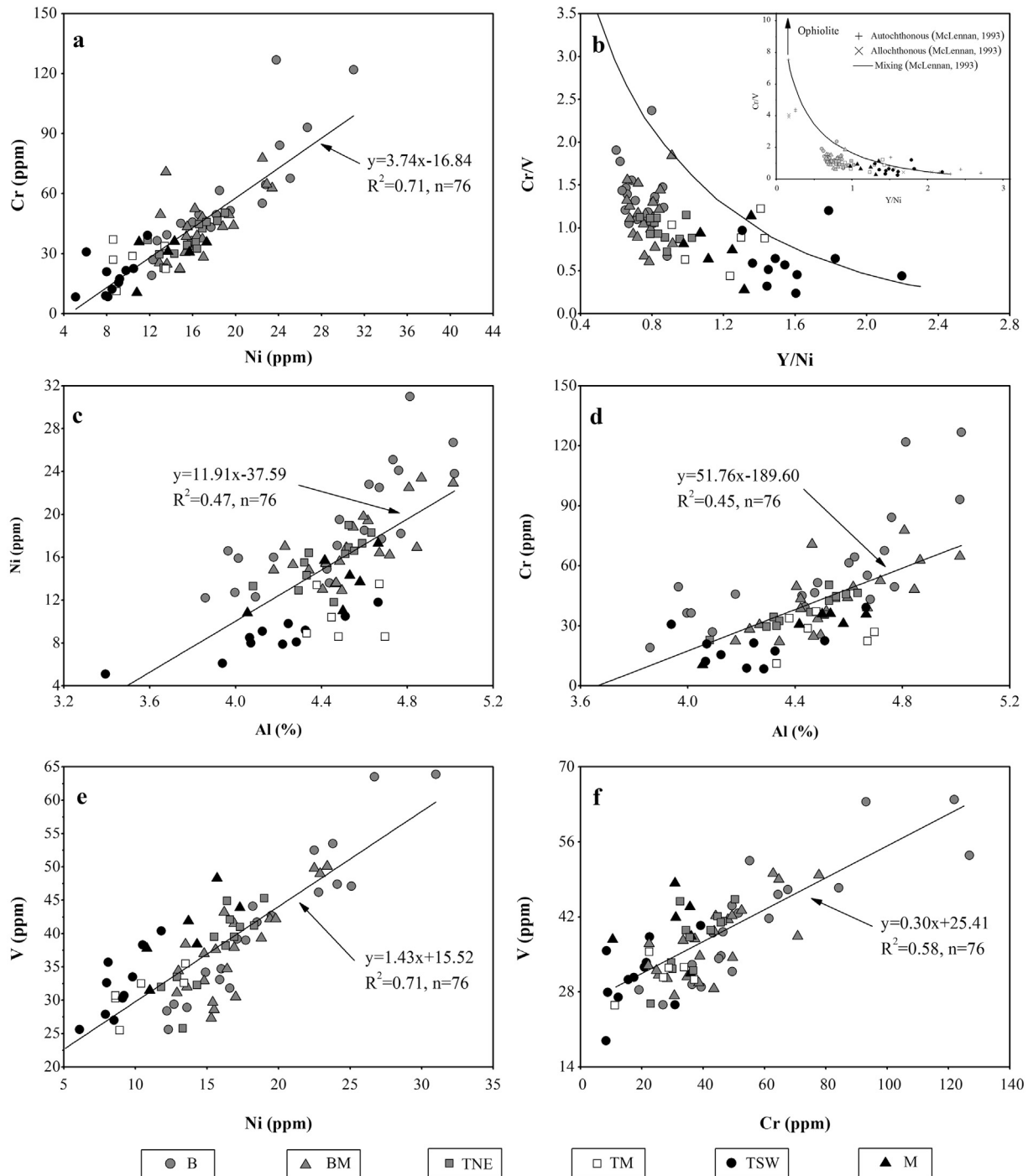


**Fig. 4.** Bivariate plots of relatively immobile elements. Cr vs. Ni (a), Ni vs. Al (c), Cr vs. Al (d), V vs. Ni (e) and V vs. Cr (f) show linear variations while plot of Cr/V vs. Y/Ni (b) shows a logarithmic distribution.

indicating minimal chemical weathering. In addition, in Fig. 10, most of the samples of the six sub-regions are near or on the weathering trendline between the UCC and terrigenous shale (Taylor and McLennan, 1985), indicating that detrital sediments from the different sub-regions have a high homogeneity in the trend of their chemical weathering. Therefore, under the low and homogeneous chemical weathering condition, the chemical difference we observed in this study may indicate a difference in provenance and composition, as seen earlier in trace elements. Similarly, in the absence of chemical weathering, the relative

contents of  $Al_2O_3$ ,  $CaO^* + Na_2O$  and  $K_2O$  are good indicators of the sediments sources in plot of A–CN–K (Nesbitt and Young, 1996). In Fig. 10, samples of B, BM and TNE align quasi-parallel with the A–CN side, unlike the more scattered TSW samples. This suggests that while TSW samples were slightly affected by K metasomatism (Fedó et al., 1995), the samples in B, BM and TNE were not.

Although the sub-region of TM is located in the east side of the oasis, its samples are chemically different from samples in both groups. In terms of elements that can be used in provenance determination, the geochemical associations between sands from



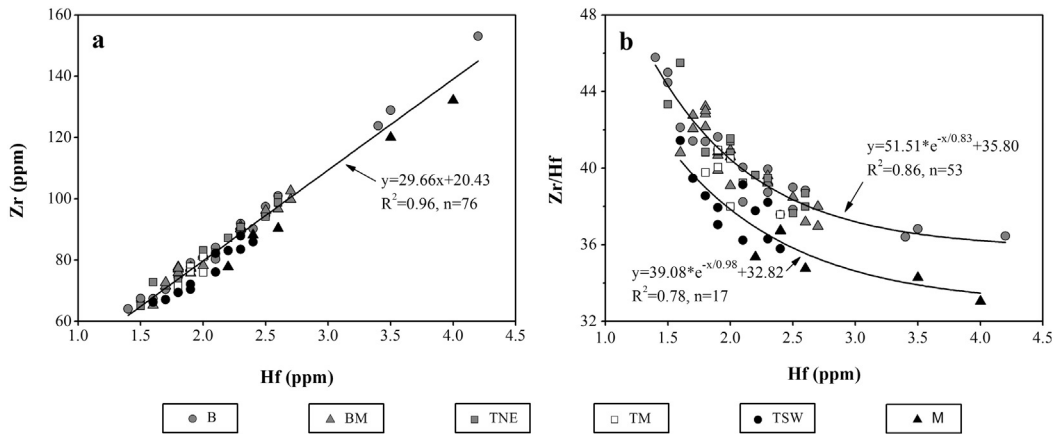


Fig. 5. (a) Plot of Zr vs. Hf, (b) plot of Zr/Hf vs. Hf with fitted exponential regression curves.

TM and the two groups are ambiguous, as they show mixed characteristics. Similarly, samples of M also show mixed characteristics. For instance, the geochemical signature of sands in TM and M fall linearly into the area between the two end members (the two groups), suggesting these sands may be a mixed product derived from these two groups (Fig. 4a, c, d, e and f). Sands of TM and M also cannot be clearly distinguished by their content variation in HFS and major elements (Figs. 5, 7, 8 and 10). The TM sub-region is located between the TNE and TSW sub-regions while the M sub-region is located between the BM and TSW sub-regions (Fig. 1). Therefore TM and M sub-regions might be affected by sediments from both of the groups, showing mixed geochemical composition. The geochemical differentiation is confirmed by the results of hierarchical cluster analysis as samples from B, BM and most of TNE (cluster A) are clearly separated from TSW samples (cluster B) (Fig. 11). M sub-region shows mixed characteristic, because some samples (42, 43, 46 and 44) belong to cluster A that represents sands from west sides of the oasis. Other samples (45 and 47) belong to cluster B2 that represent sands from TSW sub-region. As for sub-region TM, all of its samples belong to cluster B1 which represents a mixed group because it contains samples from both TSW and TNE (68, 67, and 66).

The geochemical characters of samples in west of the oasis, such as in B, BM and TNE sub-regions are homogeneous. However, samples in the east of the oasis, for example in TSW and TM sub-regions, are heterogeneous, suggesting multiple sources or multiple sediments transport processes in the east side of the oasis. Two major sediment sources for the east side of the oasis are likely: (1) sands from playas and distal fluvial deposits, (2) sands from the Tengger Desert. Deflation of sand from playas at the terminal area of the Shiyanghe River probably fed the east side of the oasis. The playas, such as Baijianhu (Fig. 1), could be easily blown by wind. Fluvial deposit supply was probably promoted by the frequent flooding of the Shiyanghe River. In this region, there was a Megalake Tengger in the Late Pleistocene (Zhang et al., 2004) as well as more recent palaeo-lakes (Feng, 1963). The ancient lacustrine sediments in the Tengger Desert and the adjacent areas of the Minqin Oasis are an important sediment source for both the oasis and the Tengger Desert. The availabilities of the aeolian sands in the surrounding areas, however, appear to have been episodic, because multiple fluvial and lacustrine sediments are present in several aeolian sections in the TNE sub-region (Pachur et al., 1995; Chen et al., 1999; Shi et al., 2002). In the closed-lake Yiema (Fig. 1), the aeolian accumulation was disconnected by lacustrine processes during ca 14,000–11,300 BP and during ca 10,000–4200 BP (Chen et al., 1999).

## 5.2. Significance of oasis in preventing desert encroachment

Wind has been recognized as a powerful agent for sediment transport in arid environments (Zimbleman et al., 1995). In the Badain Jaran Desert, the grain size of sands is mainly of fine and medium size (Yang, 1991) and thus they have the capacity to be transported by wind. In this sense, wind is the most important factor that controls the current transportation and winnowing of sands there. Good agreement between RDD values and dune orientations from many parts of the world suggest that RDD is a valuable parameter in studying dune forms and their relation to winds (Fryberger and Dean, 1979; Lancaster et al., 1987; Lancaster, 1988; Muhs et al., 1996b, 1997). The sand rose figures in this study show the RDDs are mainly from northwest to southeast (Fig. 1), indicating that sands should be transported mainly from B to BM and TNE by wind. It is also supported by the good agreement between the RDDs and the barchan dune orientations. Barchans depend on supplies of sand in unidirectional winds (Lancaster, 1995), and migrating directions parallel the prevailing wind (Bagnold, 1941). Earlier studies (Wang et al., 2007, 2008, 2009) and our field investigations found the orientations of barchans are southeastwardly in the northwest side of the Minqin Oasis. Therefore, evidence from both the geomorphology of dunes and the meteorological data indicated that the sand transport in the northwest side of the oasis is mainly controlled by wind, and the direction of the transport is towards the oasis.

The spatial distributions of K, Rb, Ba, and Sr in bulk samples are useful to further understand the aeolian sands transport processes and their implication for the evolution of aeolian sand bodies. K, Rb, and Ba are found dominantly in K-bearing minerals, particularly K-feldspar and micas (Heier and Billings, 1970; Buggle et al., 2011). Under intermediate stage of weathering, Rb and Ba are commonly retained, adsorbed on clays (Nesbitt and Young, 1984). On the basis of both theoretical calculations and laboratory experiments, it has been shown that ballistic impacts under strong (>10 m/s) winds can mechanically break sand-sized K-feldspar grains down to silt sizes (Dutta et al., 1993). Silt-sized K-feldspars can be removed from the dune field by suspension in wind, leaving a quartz-rich dune field (Muhs, 2004). Strontium is a lithophile metallic element that may replace K in a variety of rock-forming minerals including K-feldspar, gypsum, plagioclase and, especially, calcite and dolomite (Salminen et al., 2005). In this case, Sr has similar geochemical behaviors as K. Therefore, combining the spatial distribution of these elements with wind regime, is an ideal method to understand the aeolian sands transport processes. For the B, BM, and TNE regions, samples from the upwind sites in B have lower abundance of

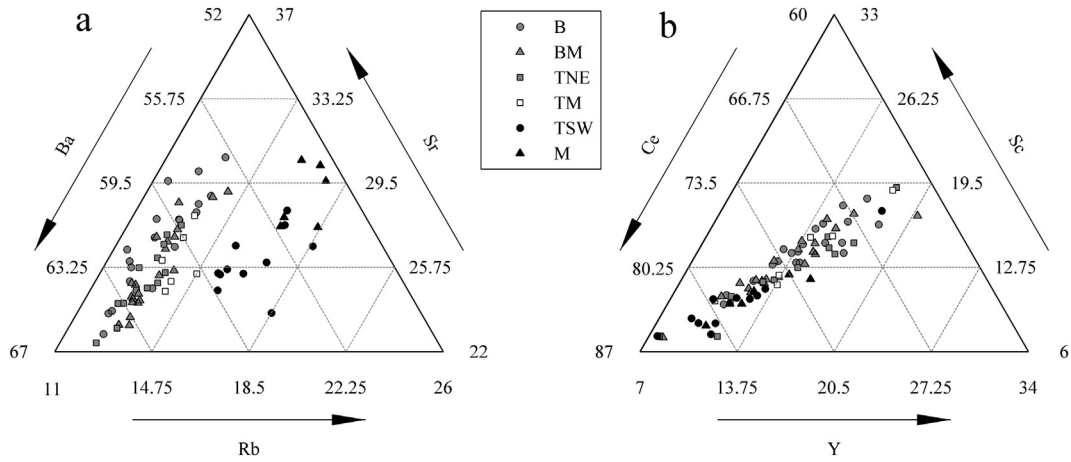


Fig. 6. Ternary plots for (a) Rb, Sr and Ba abundances (in moles) and for (b) Y, Sc, Ce abundances (in moles).

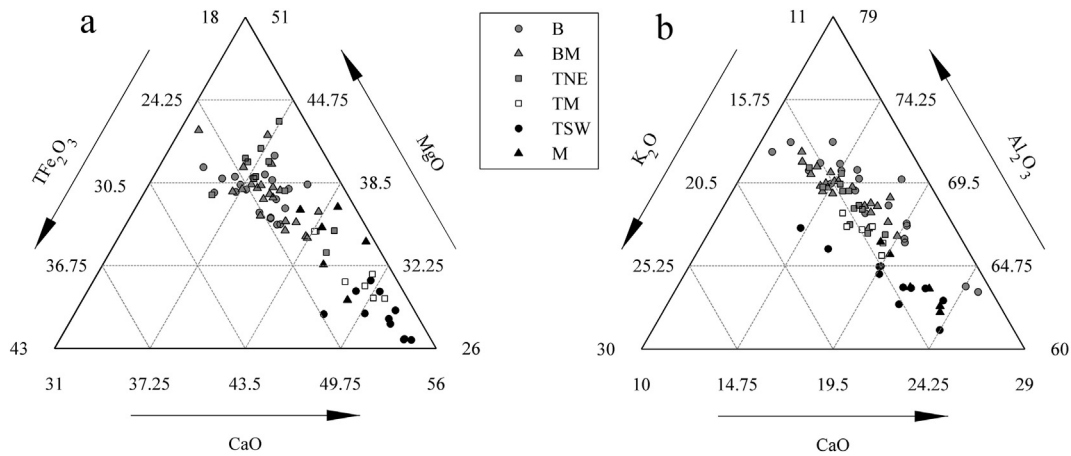


Fig. 7. Ternary plots for (a) CaO, MgO, TFe<sub>2</sub>O<sub>3</sub> abundances (in moles) and for (b) CaO, Al<sub>2</sub>O<sub>3</sub>, K<sub>2</sub>O abundances (in moles).

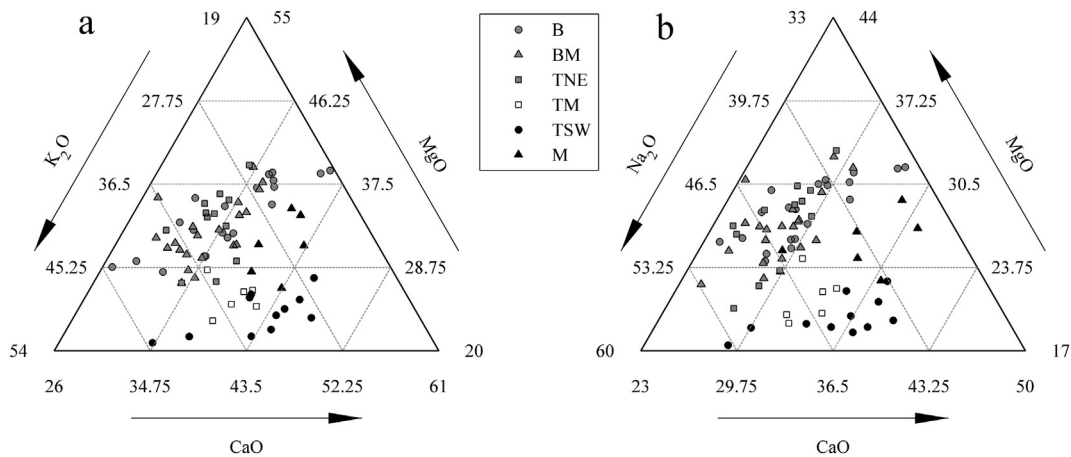


Fig. 8. Ternary plots for (a) CaO, MgO, K<sub>2</sub>O abundances (in moles) and for (b) CaO, MgO, Na<sub>2</sub>O abundances (in moles).

K, Rb, Ba, and Sr than samples in BM and TNE located downwind (Fig. 3).

The variations of selected samples in M and TSW are not in agreement with the variation of K, Rb, Ba and Sr in sub-regions B, BM and TNE (Fig. 3). This implies that although all sub-regions are characterized by similar RDP values (Fig. 1), the primary sand

transport process is not fully controlled by northwest winds. A likely reason is that the presence of the oasis causes a discontinuity of the aeolian sand transport process and leads to the different spatial distribution observed between the west and east sides of the oasis. However, sands in the oasis may come from the northwest side and therefore some of the samples from the areas of the oasis

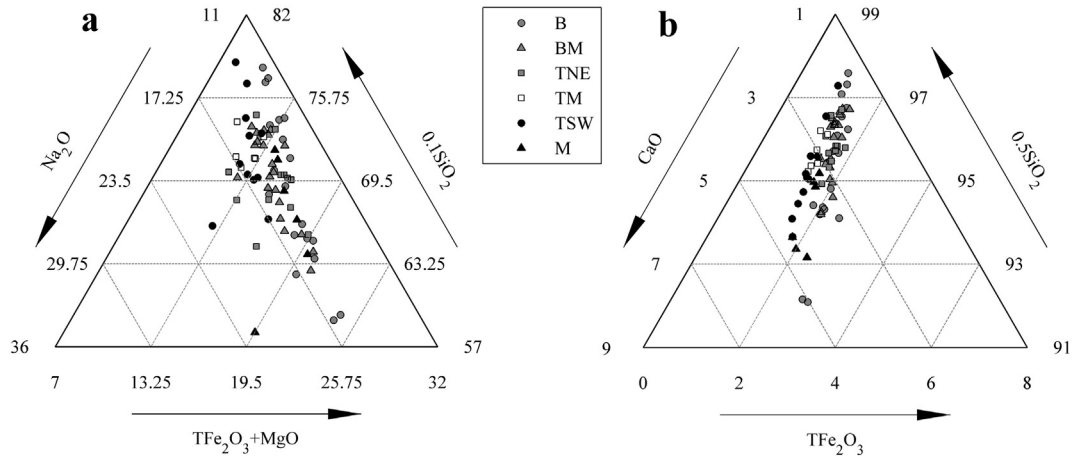


Fig. 9. Ternary plots for (a) TFe<sub>2</sub>O<sub>3</sub> + MgO, 0.1SiO<sub>2</sub> and Na<sub>2</sub>O abundances (in moles) and for (b) TFe<sub>2</sub>O<sub>3</sub>, 0.5SiO<sub>2</sub>, CaO abundances (in moles).

are more consistent with the samples taken from the Badain Jaran Desert. The spatial distributions of elements for provenance determination consistently distinguish the TSW (east side of oasis) from the B, BM and TNE (west side of oasis) (Figs. 4, 5, 6b, 7 and 8), confirming that sand in the east does not originate from the west and the oasis is an efficient barrier against sand transportation. Vegetation in the oasis plays a very important role in preventing desert encroachment, consistent with the earlier observation that the majority of sands in Chinese deserts are shifted in the surface layer (~20 cm above the ground surface, Zhu et al., 1980).

5.3. Implications for the transportation system in aeolian deposits

Smalley (1966) divided the critical events in the formation of aeolian deposits (such as loess) into three types: P provenance events, i.e. making the material; T transportation events; D deposition events, namely a PTD system. When the simple PTD system was conceived it was assumed that the interesting events were pre-deposition and the aim was to examine the P events. With growing interest in the various stages of aeolian deposit formation and

behavior, it may become necessary to introduce some sub-sections into the simple PTD system, such as the T events (Wright, 2001).

Scholars have recently emphasized the role of rivers on the transportation of loess sediments in China (Stevens et al., 2010, 2013; Smalley et al., 2014), and a fluvial–aeolian interaction in loess formation. In parallel, interests in interaction between aeolian and fluvial processes in sandy deserts are also rising (e.g., Bullard and McTainsh, 2003; Hollands et al., 2006; Yang et al., 2007a; Cohen et al., 2010; Zhu et al., 2014). Yang et al. (2007a) emphasized that not only glacial and aeolian processes but also fluvial and lacustrine processes have jointly contributed to the formation of the wide sand dunes in the Taklamakan Desert. It appears that local-scale factors such as hydrological processes and source materials, rather than regional-scale aeolian processes, are responsible for the formation of dunes in the Ejina desert (Zhu et al., 2014). These interests reflect the limitation of a single process system in understanding aeolian landform and landscape development. Our findings in this study demonstrate that oasis and related rivers in the Minqin Basin can have an important role as uncrossable obstacles for aeolian sand transportation, unlike the neighboring mountain landscape (i.e. the Yabulai Mountain).

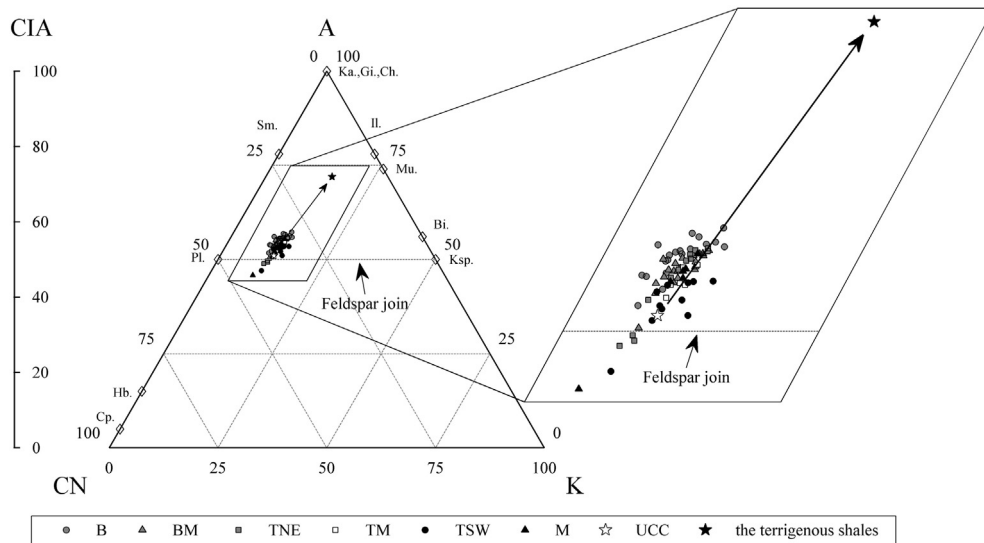
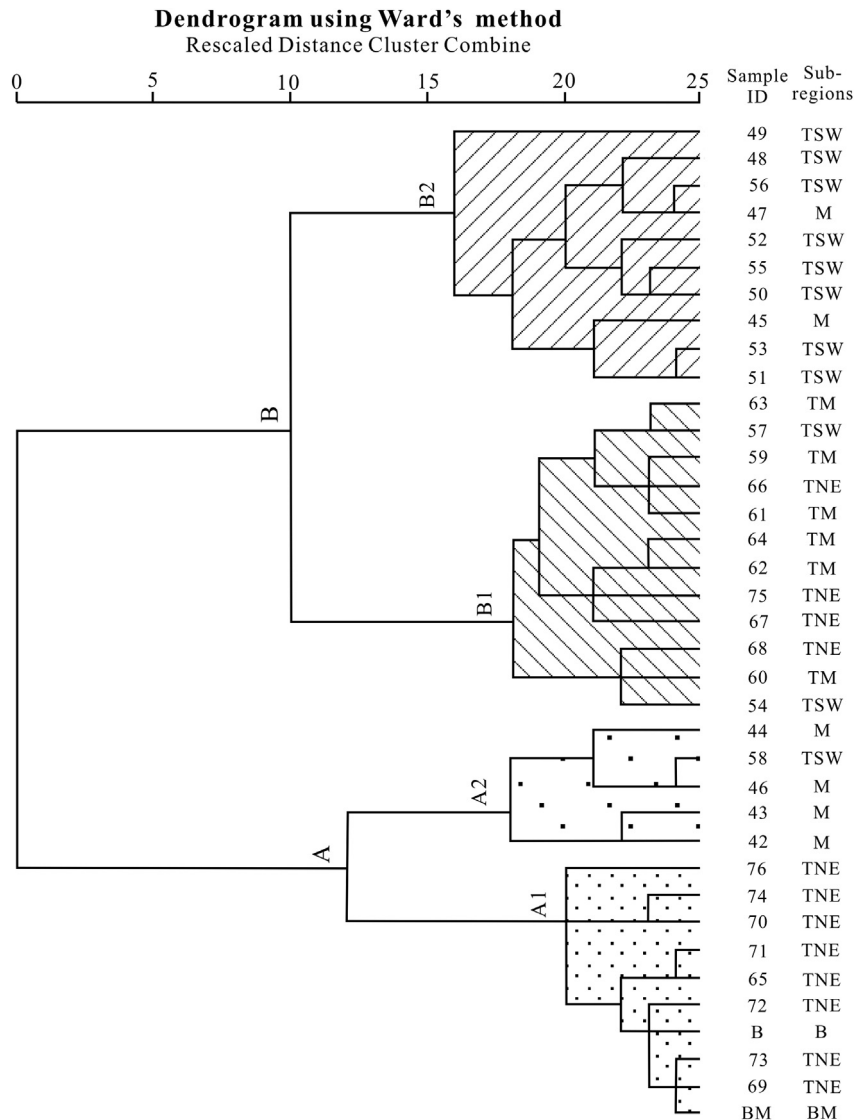


Fig. 10. A–CN–K diagram, combined with CIA values. Abbreviations: Cp = clinopyroxene; Hb = hornblende; Pl = plagioclase; Sm = smectite; Ka = kaolinite; Gi = gibbsite; Ch = chlorite; Il = illite; Mu = muscovite; Bi = biotite; Ksp = K-feldspar; A = Al<sub>2</sub>O<sub>3</sub>; K = K<sub>2</sub>O and CN = CaO + Na<sub>2</sub>O, CaO\* refers to the amount of CaO only incorporated in the silicate fraction and is calculated as for CIA.



**Fig. 11.** Dendrogram based on hierarchical clustering for 37 sample sites (for locations see Fig. 1) showing two main groups of sediments (for B and BM the average values are used).

## 6. Conclusions

Sand provenances and transport pathways can be recognized from the geochemical features of the sediments. Our geochemical data about the aeolian sands in the margins of the Badain Jaran and Tengger Deserts and the Minqin Oasis in northwestern China, supported by wind data, provided evidence for deciphering the sand sources and sand transport pathways in these regions. The spatial distribution observed in bivariate plots of Cr, Ni, Cr/V, Y/Ni, Al, V, Zr, Hf, Zr/Hf and ternary plots showed that sand sources of the northwest and southeast sides of the Minqin Oasis are different, while sands in the Oasis show mixed sources associated with sands from both sides. The spatial distribution of K, Rb, Ba and Sr as well as relatively immobile major and trace elements indicated that aeolian sands from the Badain Jaran Desert are entrained by wind, surmount the topographic obstacles, the Yabulai Mountains and the Dongda Mountains, and can reach the downwind west side of the oasis. The sands, however, do not bypass the oasis directly. The sands in the east side of the Minqin Oasis are transported by fluvial processes related to the Shiyanghe River (the major river of the

region) and by southeast winds from the Tengger Desert and the playas nearby. Our data confirm the importance of the Minqin Oasis in preventing desert encroachment.

## Acknowledgements

This collaborative research was supported by the National Natural Science Foundation of China (Grant nos.: 41172325, 11274002) and the CAS Strategic Priority Research Program (Grant no. XDA05120502). We thank the Chinese Meteorological Agency for providing weather data, Hongtao Wang for field assistance and Prof. Norm Catto and anonymous reviewers for constructive comments and suggestions.

## References

- Al-Janabi, K.Z., Ali, A.J., Al-Taie, F.H., Jack, F.J., 1988. Origin and nature of sand dunes in the alluvial plain of southern Iraq. *Journal of Arid Environments* 14, 27–34.
- Arbogast, A.F., Muhs, D.R., 2000. Geochemical and mineralogical evidence from eolian sediments for northwesterly mid-Holocene paleowinds, central Kansas, USA. *Quaternary International* 67, 107–118.



- Bagnold, R.A., 1941. *The Physics of Blown Sand and Desert Dunes*. Methuen, London.
- Bridges, C.C., 1966. Hierarchical cluster analysis. *Psychological Reports* 18, 851–854.
- Buggle, B., Glaser, B., Hambach, U., Gerasimenko, N., Marković, S., 2011. An evaluation of geochemical weathering indices in loess–paleosol studies. *Quaternary International* 240, 12–21.
- Bullard, J.E., McTainsh, G.H., 2003. Aeolian–fluvial interactions in dryland environments: examples, concepts and Australia case study. *Progress in Physical Geography* 27, 471–501.
- Canosa, F., Martin-Izard, A., Fuentes-Fuente, M., 2012. Evolved granitic systems as a source of rare-element deposits: the Ponte Segade case (Galicia, NW Spain). *Lithos* 153, 165–176.
- Chen, F., Shi, Q., Wang, J., 1999. Environmental changes documented by sedimentation of Lake Yiema in arid China since the late Glaciation. *Journal of Paleolimnology* 22, 159–169.
- Cohen, T.J., Nanson, G.C., Larsen, J.R., Jones, B.G., Price, D.M., Coleman, M., Pietsch, T.J., 2010. Late Quaternary aeolian and fluvial interactions on the Cooper Creek Fan and the association between linear and source-bordering dunes, Strzelecki Desert, Australia. *Quaternary Science Reviews* 29, 455–471.
- D'Andrade, R., 1978. U-statistic hierarchical clustering. *Psychometrika* 43, 59–67.
- Derbyshire, E., Meng, X., Kemp, R.A., 1998. Provenance, transport and characteristics of modern aeolian dust in western Gansu Province, China, and interpretation of the Quaternary loess record. *Journal of Arid Environments* 39, 497–516.
- Dinelli, E., Tateo, F., Summa, V., 2007. Geochemical and Mineralogical Proxies for Grain Size in Mudstones and Siltstones from the Pleistocene and Holocene of the Po River Alluvial Plain, Italy. *Special Papers 420*. Geological Society of America, pp. 25–36.
- Dong, Z., Man, D., Luo, W., Qian, G., Wang, J., Zhao, M., Liu, S., Zhu, G., Zhu, S., 2010. Horizontal aeolian sediment flux in the Minqin area, a major source of Chinese dust storms. *Geomorphology* 116, 58–66.
- Dutta, P.K., Zhou, Z., dos Santos, P.R., 1993. A Theoretical Study of Mineralogical Maturation of Eolian Sand. *Special Paper 284*. Geological Society of America, pp. 203–209.
- Fedo, C.M., Wayne Nesbitt, H., Young, G.M., 1995. Unraveling the effects of potassium metasomatism in sedimentary rocks and paleosols, with implications for paleoweathering conditions and provenance. *Geology* 23, 921–924.
- Feng, S., 1963. The evolution of the drainage system of the Minqin Oasis. *Acta Geographica Sinica* 29, 241–249 (in Chinese).
- Fryberger, S., Dean, G., 1979. Dune forms and wind regime. *Professional Paper 1052*. In: McKee, E. (Ed.), *A Study of Global Sand Seas*. United States Geological Survey, Washington, pp. 137–169.
- Heier, K.S., Billings, G.K., 1970. Rubidium. section 37, volume II-4. In: Wedepohl, K.H. (Ed.), *Handbook of Geochemistry*. Springer-Verlag, Berlin and Heidelberg, pp. 37C31–37N31.
- Hollands, C.B., Nanson, G.C., Jones, B.G., Bristow, C.S., Price, D.M., Pietsch, T.J., 2006. Aeolian–fluvial interaction: evidence for Late Quaternary channel change and wind–rift linear dune formation in the northwestern Simpson Desert, Australia. *Quaternary Science Reviews* 25, 142–162.
- Honda, M., Shimizu, H., 1998. Geochemical, mineralogical and sedimentological studies on the Taklimakan Desert sands. *Sedimentology* 45, 1125–1143.
- Johnson, S., 1967. Hierarchical clustering schemes. *Psychometrika* 32, 241–254.
- Kasper-Zubillaga, J.J., Acevedo-Vargas, B., Bermea, O.M., Zamora, G.O., 2008. Rare earth elements of the Altar Desert dune and coastal sands, Northwestern Mexico. *Chemie der Erde Geochemistry* 68, 45–59.
- Kocurek, G., Lancaster, N., 1999. Aeolian system sediment state: theory and Mojave Desert Kelso dune field example. *Sedimentology* 46, 505–515.
- Lancaster, N., Greeley, R., Christensen, P.R., 1987. Dunes of the Gran Desierto Sand-Sea, Sonora, Mexico. *Earth Surface Processes and Landforms* 12, 277–288.
- Lancaster, N., 1988. Development of Linear Dunes in the Southwestern Kalahari, Southern Africa.
- Lancaster, N., 1995. *Geomorphology of Desert Dunes*. Routledge, London.
- Lancaster, N., Nickling, W.G., McKenna Neuman, C., 2002. Particle size and sorting characteristics of sand in transport on the stoss slope of a small reversing dune. *Geomorphology* 43, 233–242.
- Li, X., Xiao, D., He, X., Chen, W., Song, D., 2007. Evaluation of landscape changes and ecological degradation by GIS in arid regions: a case study of the terminal oasis of the Shiyang River, northwest China. *Environmental Geology* 52, 947–956.
- Liu, T., 1985. *Loess and the Environment*. China Ocean Press, Beijing (in Chinese).
- Liu, Z.T., Yang, X.P., 2013. Geochemical-geomorphological evidence for the provenance of aeolian sands and sedimentary environments in the Hunshandake Sandy land, Eastern Inner Mongolia, China. *Acta Geologica Sinica English Edition* 87, 871–884.
- Long, H., Lai, Z., Fuchs, M., Zhang, J., Li, Y., 2012. Timing of Late Quaternary palaeolake evolution in Tengger Desert of northern China and its possible forcing mechanisms. *Global and Planetary Change* 92–93, 119–129.
- Ma, J., Wang, X., Edmunds, W.M., 2005. The characteristics of ground-water resources and their changes under the impacts of human activity in the arid Northwest China—a case study of the Shiyang River Basin. *Journal of Arid Environments* 61, 277–295.
- Ma, L., 2002. *Geological Atlas of China*. Geological Press, Beijing (in Chinese).
- McLennan, S.M., Hemming, S., McDaniel, D.K., Hanson, G.N., 1993. Geochemical approaches to sedimentation, provenance, and tectonics. In: Johnsson, M.J., Basu, A. (Eds.), *Processes Controlling the Composition of Clastic Sediments*. Geological Society of America, Boulder, Colorado, pp. 21–40. *Special Paper 284*.
- Muhs, D., Bush, C., Cowherd, S., Mahan, S., 1996a. Geomorphologic and geochemical evidence for the source of sand in the Algodones Dunes, Colorado Desert, Southeastern California. In: Tchakerian, V. (Ed.), *Desert Aeolian Processes*. Springer, Netherlands, pp. 37–74.
- Muhs, D.R., Stafford, T.W., Cowherd, S.D., Mahan, S.A., Kihl, R., Maat, P.B., Bush, C.A., Nehring, J., 1996b. Origin of the late Quaternary dune fields of northeastern Colorado. *Geomorphology* 17, 129–149.
- Muhs, D.R., Been, J., Mahan, S.A., Burdett, J., Skipp, G., Rowland, Z.M., Stafford Jr., T.W., 1997. Holocene eolian activity in the Minot dune field, North Dakota. *Canadian Journal of Earth Sciences* 34, 1442–1459.
- Muhs, D.R., Swinehart, J.B., Loope, D.B., Been, J., Mahan, S.A., Bush, C.A., 2000. Geochemical evidence for an eolian sand Dam across the North and South Platte Rivers in Nebraska. *Quaternary Research* 53, 214–222.
- Muhs, D.R., Reynolds, R.L., Been, J., Skipp, G., 2003. Eolian sand transport pathways in the southwestern United States: importance of the Colorado River and local sources. *Quaternary International* 104, 3–18.
- Muhs, D.R., 2004. Mineralogical maturity in Dune fields of North America, Africa and Australia. *Geomorphology* 59, 247–269.
- Nesbitt, H.W., Young, G.M., 1982. Early proterozoic climates and plate motions inferred from major element chemistry of lutites. *Nature* 299, 715–717.
- Nesbitt, H.W., Young, G.M., 1984. Prediction of some weathering trends of plutonic and volcanic rocks based on thermodynamic and kinetic considerations. *Geochimica et Cosmochimica Acta* 48, 1523–1534.
- Nesbitt, H.W., Young, G.M., 1996. Petrogenesis of sediments in the absence of chemical weathering: effects of abrasion and sorting on bulk composition and mineralogy. *Sedimentology* 43, 341–358.
- Pachur, H.-J., Wünnemann, B., Zhang, H., 1995. Lake evolution in the Tengger Desert, Northwestern China, during the last 40,000 years. *Quaternary Research* 44, 171–180.
- Pease, P.P., Tchakerian, V.P., Tindale, N.W., 1998. Aerosols over the Arabian Sea: geochemistry and source areas for aeolian desert dust. *Journal of Arid Environments* 39, 477–496.
- Qiao, Y., Hao, Q., Peng, S., Wang, Y., Li, J., Liu, Z., 2011. Geochemical characteristics of the eolian deposits in southern China, and their implications for provenance and weathering intensity. *Palaeogeography, Palaeoclimatology, Palaeoecology* 308, 513–523.
- Ramsey, M.S., Christensen, P.R., Lancaster, N., Howard, D.A., 1999. Identification of Sand Sources and Transport Pathways at the Kelso Dunes, California, Using Thermal Infrared Remote Sensing, vol. 111. Geological Society of America Bulletin, pp. 646–662.
- Rao, W., Chen, J., Tan, H., Jiang, S., Su, J., 2011. Sr–Nd isotopic and REE geochemical constraints on the provenance of fine-grained sands in the Ordos deserts, north-central China. *Geomorphology* 132, 123–138.
- Rollinson, H.R., 1993. *Using Geochemical Data: Evaluation, Presentation, Interpretation*. Longman Scientific & Technical Ltd., Harlow.
- Roy, P.D., Smykatz-Kloss, W., 2007. REE geochemistry of the recent playa sediments from the Thar Desert, India: an implication to playa sediment provenance. *Chemie der Erde Geochemistry* 67, 55–68.
- Ruz, M.-H., Meur-Ferec, C., 2004. Influence of high water levels on aeolian sand transport: upper beach/dune evolution on a macrotidal coast, Wissant Bay, northern France. *Geomorphology* 60, 73–87.
- Salminen, R., Batista, M.J., Bidovec, M., Demetriades, A., De Vivo, B., De Vos, W., Duris, M., Gilucis, A., Gregorauskiene, V., Halamic, J., Heitzmann, P., Lima, A., Jordan, G., Klaver, G., Klein, P., Lis, J., Locutura, J., Marsina, K., Mazreku, A., O'Connor, P.J., Olsson, S.A., Ottesen, R.-T., Petersell, V., Plant, J.A., Reeder, S., Salpeteur, I., Sandström, H., Siewers, U., Steenfelt, A., Tarvainen, T., 2005. *Geochemical Atlas of Europe. Part 1: Background Information, Methodology and Maps*. Geological Survey of Finland, Espoo.
- Shi, Q., Chen, F., Zhu, Y., Madsen, D., 2002. Lake evolution of the terminal area of Shiyang River drainage in arid China since the last glaciation. *Quaternary International* 93–94, 31–43.
- Smalley, I., 1966. The properties of glacial loess and the formation of loess deposits. *Journal of Sedimentary Petrology* 36, 669–676.
- Smalley, I., O'Hara-Dhand, K., Kwong, J., 2014. China: materials for a loess landscape. *Catena* 117, 100–107.
- Stevens, T., Palk, C., Carter, A., Lu, H., Clift, P.D., 2010. Assessing the Provenance of Loess and Desert Sediments in Northern China Using U–Pb Dating and Morphology of Detrital Zircons, vol. 122. Geological Society of America Bulletin, pp. 1331–1344.
- Stevens, T., Carter, A., Watson, T.P., Vermeesch, P., Andò, S., Bird, A.F., Lu, H., Garzanti, E., Cottam, M.A., Sevastjanova, I., 2013. Genetic linkage between the Yellow River, the Mu Us desert and the Chinese Loess Plateau. *Quaternary Science Reviews* 78, 355–368.
- Sun, J., 2002. Provenance of loess material and formation of loess deposits on the Chinese Loess Plateau. *Earth and Planetary Science Letters* 203, 845–859.
- Tang, Q., Qu, Y., Zhou, J., 1992. *The Hydrology and Water Resources Used in Arid Areas of China*. Science Press, Beijing (in Chinese).
- Taylor, S.R., McLennan, S.M., 1985. *The Continental Crust: Its Composition and Evolution*. Blackwell Scientific Publications, London.
- Templ, M., Filzmoser, P., Reimann, C., 2008. Cluster analysis applied to regional geochemical data: problems and possibilities. *Applied Geochemistry* 23, 2198–2213.
- Toar, H., White, B., Berman, E., 1996. The effect of slopes on sand transport – numerical modelling. *Landscape and Urban Planning* 34, 171–181.
- Ujvari, G., Varga, A., Balogh-Brunstad, Z., 2008. Origin, weathering, and geochemical composition of loess in southwestern Hungary. *Quaternary Research* 69, 421–437.

- Villatoro, M.M., Amos, C.L., Umgiesser, G., Ferrarin, C., Zaggia, L., Thompson, C.E.L., Are, D., 2010. Sand transport measurements in Chioggia inlet, Venice lagoon: theory versus observations. *Continental Shelf Research* 30, 1000–1018.
- Wang, X., Griffin, W.L., Chen, J., 2010. Hf contents and Zr/Hf ratios in granitic zircons. *Geochemical Journal* 44, 65–72.
- Wang, Z., Tao, S., Xie, Y., Dong, G., 2007. Barchans of Minqin: morphometry. *Geomorphology* 89, 405–411.
- Wang, Z., Zhang, J., Zhang, Q., Qiang, M., Chen, F., Ling, Y., 2008. Barchans of Minqin: sediment transport. *Geomorphology* 96, 233–238.
- Wang, Z., Zhao, H., Zhang, K., Ren, X., Chen, F., Wang, T., 2009. Barchans of Minqin: quantifying migration rate of a barchan. *Sciences in Cold and Arid Regions* 1, 151–156.
- Ward, J.H., 1963. Hierarchical grouping to optimize an objective function. *Journal of the American Statistical Association* 48, 236–244.
- Wolff, D.D., Parsons, M.L., 1983. *Pattern Recognition Approach to Data Interpretation*. Plenum Press, New York.
- Wopfner, H., Twidale, C.R., 1988. Formation and age of desert dunes in the Lake Eyre epicentres in central Australia. *Geologische Rundschau* 77, 815–834.
- Wright, J.S., 2001. "Desert" loess versus "glacial" loess: quartz silt formation, source areas and sediment pathways in the formation of loess deposits. *Geomorphology* 36, 231–256.
- Xue, J., Lee, C., Wakeham, S.G., Armstrong, R.A., 2011. Using principal components analysis (PCA) with cluster analysis to study the organic geochemistry of sinking particles in the ocean. *Organic Geochemistry* 42, 356–367.
- Yang, X., 1991. *Geomorphologische Untersuchungen in Trockenräumen NW-Chinas unter besonderer Berücksichtigung von Badanjinlin und Takelamagan*. Göttinger Geographische Abhandlungen 96, 1–124.
- Yang, X., Rost, K.T., Lehmkühl, F., Zhenda, Z., Dodson, J., 2004. The evolution of dry lands in northern China and in the Republic of Mongolia since the Last Glacial Maximum. *Quaternary International* 118–119, 69–85.
- Yang, X., Zhu, B., White, P.D., 2007a. Provenance of aeolian sediment in the Taklamakan Desert of western China, inferred from REE and major-elemental data. *Quaternary International* 175, 71–85.
- Yang, X., Liu, Y., Li, C., Song, Y., Zhu, H., Jin, X., 2007b. Rare earth elements of aeolian deposits in Northern China and their implications for determining the provenance of dust storms in Beijing. *Geomorphology* 87, 365–377.
- Yang, X., Ma, N., Dong, J., Zhu, B., Xu, B., Ma, Z., Liu, J., 2010. Recharge to the interdune lakes and Holocene climatic changes in the Badain Jaran Desert, western China. *Quaternary Research* 73, 10–19.
- Yang, X., Scuderi, L., Paillou, P., Liu, Z., Li, H., Ren, X., 2011. Quaternary environmental changes in the drylands of China – a critical review. *Quaternary Science Reviews* 30, 3219–3233.
- Yang, X., Li, H., Conacher, A., 2012. Large-scale controls on the development of sand seas in northern China. *Quaternary International* 250, 74–83.
- Yang, X., Wang, X., Liu, Z., Li, H., Ren, X., Zhang, D., Ma, Z., Rioual, P., Jin, X., Scuderi, L., 2013. Initiation and variation of the dune fields in semi-arid China – with a special reference to the Hunshandake Sandy Land, Inner Mongolia. *Quaternary Science Reviews* 78, 369–380.
- Ye, D., 1990. *Study on Possible Future Global Changes in China*. Meteorological Press, Beijing (in Chinese).
- Zhang, H., Ma, Y., Li, J., Qi, Y., Chen, G., Fang, H., Wünnemann, B., Pachur, H.-J., 2001. Palaeolake evolution and abrupt climate changes during Last Glacial Period in NW China. *Geophysical Research Letters* 28, 3203–3206.
- Zhang, H., Wünnemann, B., Ma, Y., Peng, J., Pachur, H.-J., Li, J., Qi, Y., Chen, G., Fang, H., Feng, Z., 2002. Lake Level and climate changes between 42,000 and 18,000 <sup>14</sup>C yr B.P. in the Tengger Desert, Northwestern China. *Quaternary Research* 58, 62–72.
- Zhang, H., Peng, J., Ma, Y., Chen, G., Feng, Z., Li, B., Fan, H., Chang, F., Lei, G., Wünnemann, B., 2004. Late Quaternary palaeolake levels in Tengger Desert, NW China. *Palaeogeography, Palaeoclimatology, Palaeoecology* 211, 45–58.
- Zhang, K., Qu, J., Zu, R., Fang, H., 2005. Temporal variations of sandstorms in Minqin oasis during 1954–2000. *Environmental Geology* 49, 332–338.
- Zhang, X., Wang, X., Yan, P., 2008. Re-evaluating the impacts of human activity and environmental change on desertification in the Minqin Oasis, China. *Environmental Geology* 55, 705–715.
- Zhu, B., Yang, X., 2009. Chemical weathering of detrital sediments in the Taklamakan Desert, Northwestern China. *Geographical Research* 47, 57–70.
- Zhu, B., Yu, J., Rioual, P., Ren, X., 2014. Particle size variation of aeolian dune deposits in the lower reaches of the Heihe River basin, China. *Sedimentary Geology* 301, 54–69.
- Zhu, Z., Wu, Z., Liu, S., Di, X., 1980. *An Outline of Chinese Deserts*. Science Press, Beijing (in Chinese).
- Zimbelman, J.R., Williams, S.H., Tchakerian, V.P., 1995. Sand transport paths in the Mojave Desert, Southwestern United States. In: Tchakerian, V.P. (Ed.), *Desert Aeolian Processes*. Chapman and Hall, London, pp. 101–129.
- Zimbelman, J.R., Williams, S.H., 2002. Geochemical Indicators of Separate Sources for Eolian Sands in the Eastern Mojave Desert, California, and Western Arizona, vol. 114. *Geological Society of America Bulletin*, pp. 490–496.